AUSTRALIS: A new tool for the study of isotopic systems and geochronology in mineral systems

S. H. Sie[a]; T. R. Niklaus[ab]; D. A. Sims[ac]; F. Bruhn[ad]; G. Suter[a]; G. Cripps[a]

[a] Australian Geodynamics Cooperative Research Centre, Heavy Ion Analytical Facility, CSIRO Exploration and Mining, North Ryde, NSW, Australia [b] Credit Suisse, CIC, Zurich, Switzerland [c] RLM Systems, East Burwood, Vic., Australia [d] Leibniz Laboratory, Christian Albrechts University, Kiel, Germany

PLEASE SCROLL DOWN FOR ARTICLE

AUSTRALIS: a new tool for the study of isotopic systems and geochronology in mineral systems

S. H. SIE,* T. R. NIKLAUS,[†] D. A. SIMS,[‡] F. BRUHN,[§] G. SUTER AND G. CRIPPS

Australian Geodynamics Cooperative Research Centre, Heavy Ion Analytical Facility, CSIRO Exploration and Mining, PO Box 136, North Ryde, NSW 2113, Australia.

AUSTRALIS (*AMS* for *Ul*tra *S*ensitive *TRA*ce e*L*ement and *I*sotopic *St*udies) is a microbeam accelerator mass spectrometry (AMS) system designed for *in situ* microanalysis of geological samples for trace elements and radiogenic and stable isotope data. The AMS method eliminates molecular and isobaric interferences in *in situ* mass spectrometric measurements, opening up new opportunities in geochronology and tracer applications. Tests have been carried out for measurements of Pb, S and Os isotopes, conducted mainly at 1.5 MV accelerating voltage. In Pb and S tests, precision as high as 0.3‰ has been obtained, made possible by a fast isotope switching system to counter the effect of instabilities in the ion source and beam transport system. In trace-element analysis, a detection limit for Au at the sub-ppb level was obtained.

KEY WORDS: accelerator mass spectrometry, isotope geology, microanalysis, trace elements.

INTRODUCTION

Isotopic and trace-element data are often crucial for constraining interpretation of petrological data, being one of a number of latent signatures of geological processes from magma generation, differentiation and subsequent evolution by metasomatic and metamorphic events. While whole-rock data can be sufficient, the significance and magnitude of expression are enhanced on selected species of the mineral constituent, arising from special properties (e.g. resistance to weathering, stability against certain processes or being the preferred species for concentration of elements of interest). To obtain data from specific minerals, mineral separation is necessary. For precise isotopic data, this is often followed by chemical extraction prior to mass spectrometric analysis.

The advent of *in situ* microbeam methods obviated the need for this elaborate, tedious sample treatment. More importantly, these methods enable the analysis of complex intergrown phases (in which mineral separation is impractical or simply unfeasible), fine structure in minerals (such as growth zones), microscopic melt and fluid inclusions. The two foremost methods are secondary ion mass spectrometry (SIMS) using the ion microprobe (see Reed 1989 for a review) and laser ablation sampling followed by inductively coupled plasma source mass spectrometry (ICP-MS) (Reed 1990; Walder *et al.* 1993). However, in these methods molecular ions are inevitably produced even from a simple matrix that can interfere with the atomic ions of interest, giving rise to what is termed molecular interference. Isobaric interference arising from atomic ions from a different atomic species having the same weight number can also compound the problem. Some of this can be resolved by invoking a high mass resolution in the spectrometer, pioneered by the Sensitive High Resolution Ion Microprobe (SHRIMP) (Compston *et al.* 1982) and joined later by the Cameca IMS1270. These successfully eliminated the problem of molecular interference even at the high mass region (e.g. Pb) and some isobaric interference in the lower mass region. However, for the medium to heavy mass region isobaric interference resolution requires extremely high mass resolution. For example, to resolve ^{87}Sr from the parent nucleus ^{87}Rb a mass resolution >40 000 is required. To achieve such high resolution presents a considerable technical challenge.

Accelerator mass spectrometry (AMS) presents an alternative approach for eliminating or suppressing these molecular and isobaric interferences. The principle of the method is illustrated in Figure 1. In essence, the method is double mass spectrometry, in which the first stage is a negative ion SIMS, followed by further acceleration of the ions in a tandem electrostatic accelerator, before the final analysis in the second mass spectrometer. The accelerator acts as a molecular disintegrator eliminating most mass interference problems without resorting to high mass resolution, and with an efficiency comparable to single stage mass spectrometry. For example, in radiocarbon measurements, an overall detection efficiency of ~3.3% is obtained for 3+ ions (Sie *et al.* 1997).

In a tandem accelerator, acceleration occurs in two stages. The first stage requires negative ions for acceleration through attraction by the positively charged high-voltage terminal. In the terminal the negative ions pass through a 'stripper canal', a tube filled with argon gas at a few hundred Pascals pressure. Molecular ions are

---

*Corresponding author: Soey.Sie@csiro.au
[†]Present address: Credit Suisse, CIC, Postfach 100, 8070 Zurich, Switzerland.
[‡]Present address: RLM Systems, 23 Lakeside Drive, East Burwood, Vic. 3151, Australia.
[§]Present address: Leibniz Laboratory, Christian Albrechts University, Max-Eyth St. 11-13, 24118 Kiel, Germany.

destroyed in this process due to Coulomb explosion following multiple electron stripping through collisions with the gas atoms. The second stage of acceleration to ground potential occurs when these ions are repulsed by the terminal voltage. The total energy gained by the ions in MeV units is $E = \delta + (1 + q)V$, where δ is the ion source extraction energy (in MeV), q the charge state of the positive ion in electronic charge units and V the terminal voltage in MV. For injection of molecular ions with
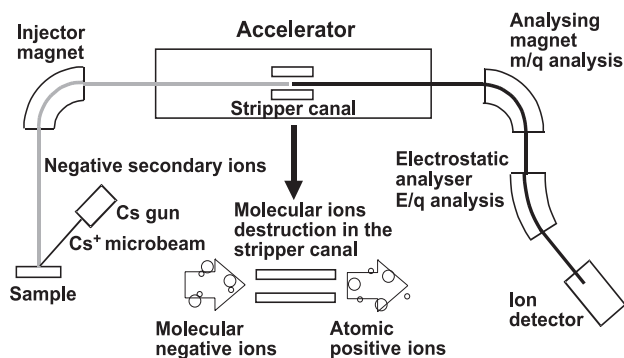

Figure 1 Principle of accelerator mass spectrometry (AMS). A Cs$^+$ primary beam produces negative secondary ions from the sample, which are first extracted at ~10 kV voltage, followed by selection of the ions of interest in the injector magnet. These are accelerated through the tandem accelerator and converted to positive ions in the stripper canal inside the high-voltage terminal. Molecular ions are disintegrated into their atomic constituents and these atomic ions are then analysed in the high-energy side using both magnetic and electrostatic analysis before detection in the ion detector.

molecular weight M, and atomic fragment of interest m, the energy is given by $E = \mu\delta + (\mu + q)V$, where $\mu = m/M$. The atomic ions can be resolved at moderate mass resolution.

The negative secondary ions are generated from the sample by sputtering using a Cs$^+$ beam. The use of negative ions from the source, as in SIMS, can be exploited to reduce or eliminate isobaric interference. For example ^{14}N$^-$ is unstable and hence does not interfere with ^{14}C$^-$, and Re$^-$ ion production is ~200× less than Os$^-$, reducing the interference on ^{187}Os. More importantly, AMS can exploit the availability of a variety of molecular ions to achieve the same end. For example Rb interference can be reduced by deliberately selecting Sr hydride ions in ^{87}Sr measurements.

The isotopes of interest are measured sequentially. In the first stage, isotope switching is achieved by energy modulation through a static magnetic field. At the high-energy side, isotope switching in the second mass spectrometer is based on a beam-deflecting system operated synchronously with that at the low-energy side. The isotope switching can be driven at a high rate (<1 msec/isotope), which may be required to achieve high precision in the isotopic ratio measurements.

Accelerator mass spectrometry has been applied almost exclusively to measurements of cosmogenic nuclei and in most of these applications precision in the per cent regime is often adequate. For general isotope geology, this precision has to be improved by at least 10-fold. However, even when this is achieved, bulk AMS is not competitive against TIMS in which interference problems are eliminated through chemical processing of the sample. For effective application as an *in situ* method, AMS must be applied as a
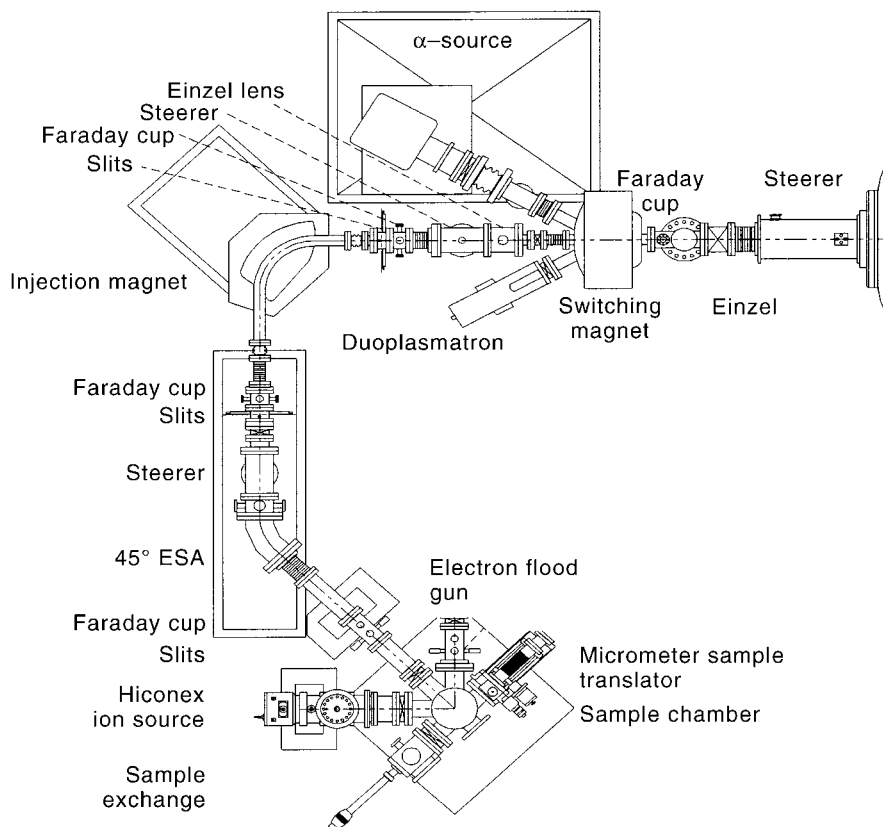
Figure 2 The injector system of AUSTRALIS, comprised of the sample chamber and the low-energy analysing system, consisting of a 30 cm radius spherical electrostatic analyser and a 30 cm radius, 90° bend magnet. Ions can be analysed at the image point of the magnet as current or pulse counting. Sequential injection of isotopes at constant magnetic field is carried out by modulating the beam energy by applying appropriate voltages to the electrically isolated injection magnet beam box.

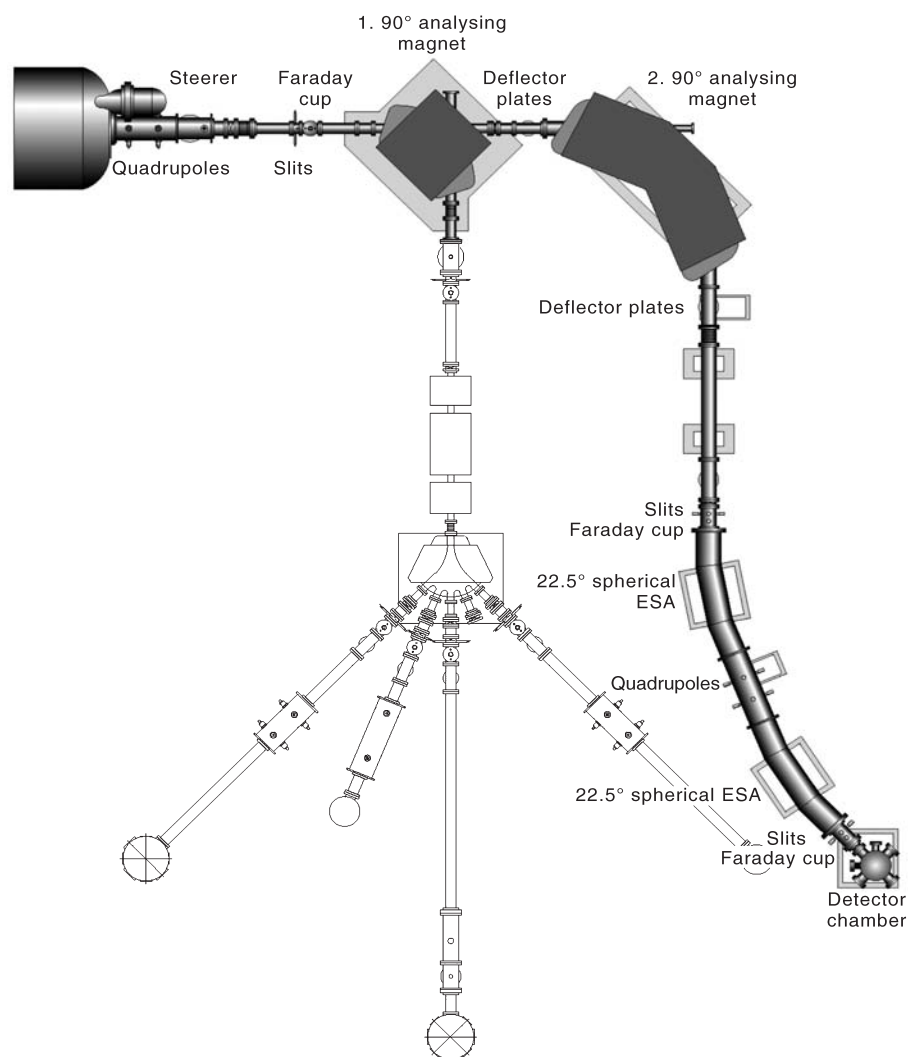**Figure 3** The high-energy mass spectrometer system, incorporating a 90° bend dipole magnet corrected to the second order, followed by two 22.5° bend spherical electrostatic analysers separated by a quadrupole doublet. The high-energy isotope switching system consists of two pairs of electrostatic deflectors at the entrance and exit of the magnet, deflecting the beam in the orbit plane.

microbeam technique. This motivated the development of a microbeam AMS system at the CSIRO Heavy Ion Analytical Facility (HIAF) in Sydney (Sie *et al.* 1997), known as AUSTRALIS (*A*MS for *U*ltra *S*ensitive *TRA*ce e*L*ement and *I*sotopic *S*tudies). It is designed to enable microanalysis of mineralogical samples for isotopic data in general, and is virtually unrestricted by molecular and isobaric interferences.

AUSTRALIS

The AUSTRALIS system is designed to deliver the advantages of AMS as an *in situ* microanalytical method, and with efficiency for large-scale, high-throughput applications suitable for exploration research applications. To this end, considerable attention was paid to the design of the sample chamber.

The chamber features a zoom microscope-based sample-viewing system in the reflected geometry, facilitating visual tuning and positioning of the primary microbeam. The ion source produces a 30 μm diameter Cs^+ beam routinely. Samples are mounted on a three-axis microstage

with a 0.5 μm minimum step-size, computer driven through a graphic interface. The sample holder accommodates three 25 mm diameter samples, or two thin-sections, which can be exchanged quickly through a vacuum lock.

The Cs^+ beam strikes the sample at 45° incidence and the negative secondary ion beam is extracted at a normal angle to the sample. An electron flood gun, mounted at the opposite 45° angle, is used to compensate charge buildup during the analysis of insulating samples. The injector system, comprised of the sample chamber and the 'low energy' beam transport system is shown in Figure 2. The secondary ions are first focused using an immersion einzel lens to form an object for a 45° bend, 30 cm mean radius, 2.5 cm gap spherical electrostatic analyser (ESA), set in a double focusing configuration. The image in turn becomes the object for a 90° bend, 30 cm mean radius, 3 cm gap double focusing analysing magnet. The magnet box is insulated to allow application of modulating voltages to vary the beam energy. This enables rapid sequential injection of the different isotopes at a fixed magnetic field, a method known commonly as the 'bouncing' method. The analysed ion beam can be monitored at the focal point of the magnet in either a Faraday cup or an ETP electron

multiplier acting as an ion counter. Coupled to a fast pulse amplifier, the ion counter can be driven at a counting rate as high as ~10 MHz, giving a good overlap with current measurements in which the noise level is at ~0.1 pA, which corresponds to ~0.6 Mhz count rate for a singly charged ion. To minimise dead time correction, the counter is usually run at less than 1 Mhz.

After acceleration and conversion to positive, elemental ions, the beam enters a 90° bend, 1.3 m mean radius, 2.5 cm gap magnet, corrected to the 2nd order, with a beam product of 140 MeV.amu, operated in the double focusing, unity magnification mode. This 'high energy' beam transport system comprising the high energy mass spectrometer is shown in Figure 3. Two pairs of electrostatic deflector plates at the entrance and exit ports of the magnet box, deflecting the beam in the orbit plane, comprise the bouncing system for the high energy. The magnet is followed by
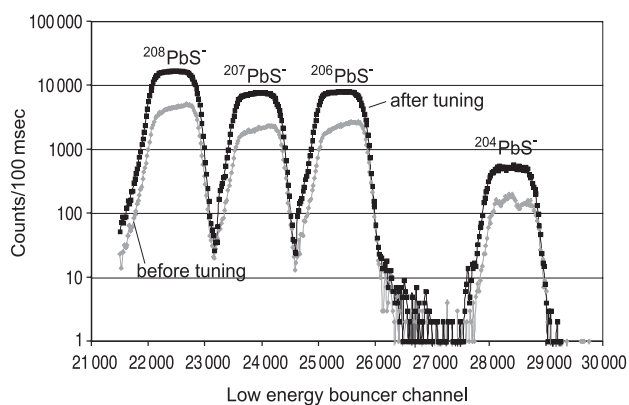
two 3 m mean radius, 2.5 cm gap, 22.5° bend spherical ESA, separated by a doublet electrostatic quadrupole that focuses the beam into the detector chamber. The ions can be detected in either a Faraday cup, a gas proportional counter or an electron multiplier based ion counter (ETP counter).

At 1.5 MV terminal voltage, typical charge multiplication, defined as the (positive) current at the high energy divided by the injected (negative) current, is ~2.5 for a heavy ion (e.g. Pb) beam. For ~100 pA injected beam, typical yield for the 3+, 4+ and 5+ ions are 16, 4 and 1 pA, respectively. The yield for 5+ ions is expected to almost double, whereas the 3+ yield is relatively flat by increasing the terminal voltage from 1.5 to 2 MV. In terms of particle yield, it is more advantageous to use the lower charge state, being the more prolific one, except that choice may be limited by insufficient analysing magnet field strength and the possibility of incomplete Coulomb explosion. We have selected the 4+ ions for Pb and 2+ for S at 1.5 MV terminal voltage in most measurements as being optimum.

RESULTS

Measurements to date have been reconnaissance in nature and research effort has been concentrated on assessing a selection of isotopic systems and improving the precision in isotopic ratio measurements. To date we have investigated the Pb, S and Os isotopes, covering contrasting conditions necessitating different approaches.

Pb isotopes

AUSTRALIS offers the prospect of carrying out Pb isotope measurements in minerals in which mass interference by hydride ions is expected due to the presence of hydroxyl in the sample (e.g. ^{208}Pb by ^{207}PbH or ^{206}PbH$_2$, ^{207}Pb by ^{206}PbH). These can, in principle, be resolved in conventional mass spectrometry with a mass resolution of the order 20 000. However, apart from the technical difficulty in achieving such a resolution, the efficiency of such

Figure 4 Mass spectrum of PbS⁻ ions from galena measured in the ion counter at the low-energy magnet image point, by scanning the low-energy bouncer (modulating voltage). Note that the mass scale descends with higher bouncer channels. The intrinsic mass resolution is ~850, but the image slits are widened to achieve 'flat-top' transmission. The flat part of the peak is a sensitive diagnostic tool for tuning the injector. Skewness can be corrected by adjusting the beam transport parameters and/or extraction voltage.
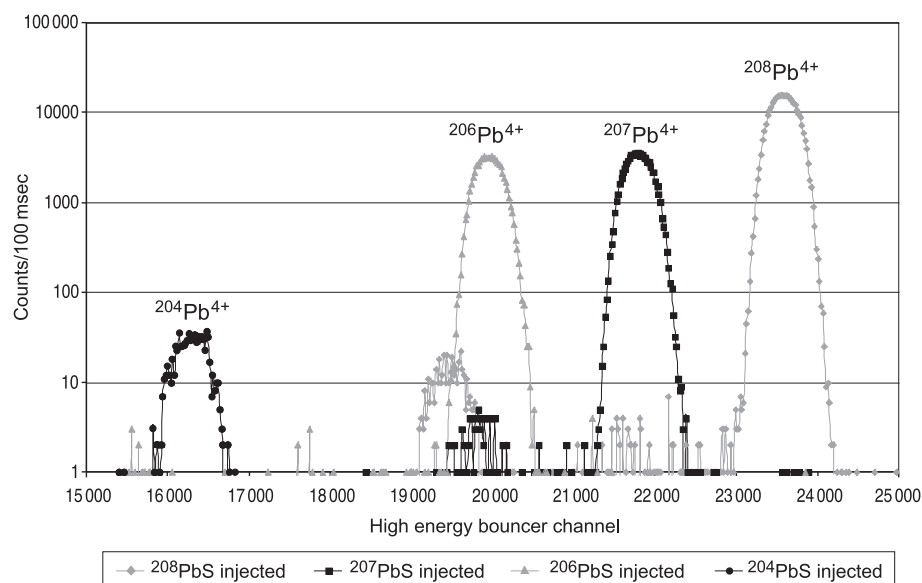

Figure 5 Composite mass spectra of Pb⁴⁺ ions measured in the high-energy ion counter for various injected PbS⁻ ions. For injected mass 240 ion corresponding to mainly ^{208}Pb^{32}S⁻, the dominant ^{208}Pb⁴⁺ peak is well separated from other Pb⁴⁺ isotopes, fragments of the interfering molecules ^{207}Pb^{33}S⁻, ^{207}Pb^{32}SH⁻ and ^{206}Pb^{34}S⁻. Similarly, ^{207}Pb⁴⁺, ^{206}Pb⁴⁺ and ^{204}Pb⁴⁺ ions, respectively, are the dominant peak when mass 239, 238 and 237 are injected.

measurements would be inherently low. With AMS, these interfering molecules would be eliminated as a matter of course.

We have chosen galena as our test sample for common Pb isotope measurements. Although Pb is a major element in the sample, the PbS^- and PbS_2^- ions are two orders of magnitude more prolific than the Pb^- ions. The PbS^- ions were selected for the measurements, and serve as an illustration of one of the advantages of AMS, namely the ability to exploit molecular ions. PbO^- ions are also produced from this sample, and in fact are stronger than the Pb^- ions, even though only a trace amount of oxygen is present due to residual air in the vacuum system. This peak can presumably be exploited in Pb measurements from silicates.

The mass spectrum of the secondary ions is first measured at the image point of the low-energy magnet. The mass range is unrestricted when measured by scanning the magnetic field, but for the actual measurement, a finite mass region of interest is measured by fixing the magnetic field and scanning the bouncing voltage. With all slits open and the magnet image slits set at 300 μm, a mass resolution of ~850 is obtained routinely for beam spot sizes between 30 and 100 μm. The magnet image slits are usually widened to allow 'flat top' transmission to reduce the effect of energy drift in the beam. Figure 4 shows such a spectrum from galena obtained using the ion counter in the mass region of interest showing the $Pb^{32}S^-$ as the strongest peaks. The mass 240 peak contains mainly $^{208}Pb^{32}S^-$ (labelled 208 in Figure 4), ~4% $^{206}Pb^{34}S^-$, ~0.8% $^{207}Pb^{33}S^-$ and possibly $^{207}Pb^{32}SH^-$ peaks. The flat part of the peak is a sensitive diagnostic tool for tuning the low-energy beam-transport system, specifically the alignment of the orbit with the true optical axis. Skewness of the peak can be corrected
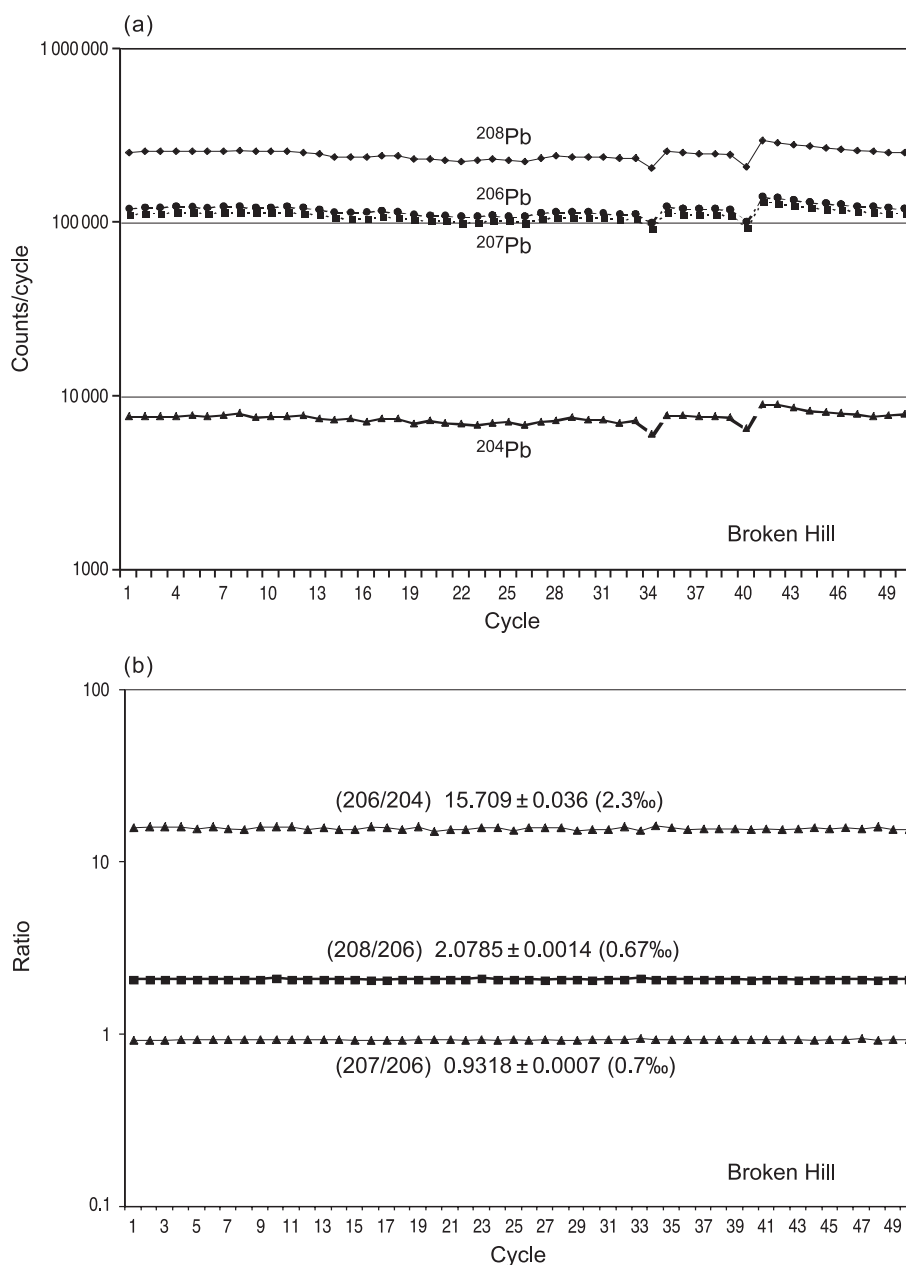

Figure 6 (a) Pb^{4+} ions detected at the high-energy end. Each point represents 200 cycles of 5 msec counting per isotope. The measurements show the instability of the beam intensity, but fast cycling reflects this instability in all isotopes. (b) Isotopic ratios obtained from data in (a). The fast cycling eliminates the effect of beam fluctuation, resulting in high precision.

by adjusting the beam-transport parameters and the secondary extraction voltage.

The accelerator is tuned to achieve overlap of the mass spectra measured in the high energy and in the low energy Faraday cups, ensuring maximum transmission efficiency. The high-energy magnet is set to pass $^{206}Pb^{4+}$ from $^{206}Pb^{32}S^-$ and the high-energy bouncer scanned to cover ~3 mass units on either side. Figure 5 shows the mass spectra measured at the high-energy ion counter for injected masses of 240, 239, 238 and 236. The spectrum corresponding to mass 240 injection shows the dominant $^{208}Pb^{4+}$, which is clearly resolved from the $^{206}Pb^{4+}$ and $^{207}Pb^{4+}$ peaks, fragments of the interfering molecules. Similarly, the spectra corresponding to injected mass of 239, 238 and 236 show the $^{207}Pb^{4+}$, $^{206}Pb^{4+}$ and $^{204}Pb^{4+}$ peaks, respectively as the dominant peaks. The peaks are only slightly flat topped because the beam size at this point is just under the aperture size of the ion counter.

For ratio measurements, the isotopes are detected sequentially by synchronising the low-energy and high-energy bouncer settings cyclically. For example, the high-energy bouncer is set to detect $^{208}Pb^{4+}$ when injecting mass 240, $^{207}Pb^{4+}$ when injecting mass 239 and so on. Beam stability directly affects precision, and the sputtering process as well as instabilities in the beam-transport system are the main sources of fluctuation. By cycling through the isotopes faster than the period of the instabilities, precision can be improved. Initially the switching rate was limited to >150 msec/isotope by the software-based bouncer driver, which limited the precision to per cent levels. This was replaced with a hardware-based bouncer system that permits switching time as low as 1 msec/isotope. Our experience indicated that the effect of beam fluctuations on isotopic ratios is reduced significantly at less than 10 msec/isotope switching time. Figure 6a shows the Pb^{4+} isotopes detected at the high-energy side as a function of time, from injected PbS^-. Each point corresponds to 200 cycles of 5 msec counting time. With fast cycling, beam instabilities are reflected in all isotopes,
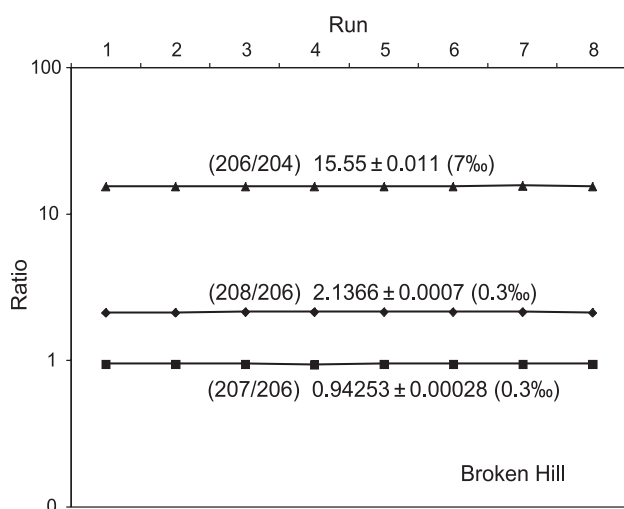
minimising the effect and resulting in high precision in the isotopic ratios (Figure 6b). Repeat measurements (Figure 7) of the Pb isotopic ratios from a galena sample from Broken Hill, show very little variation in the $^{207}Pb/^{206}Pb$ ratio taken at different analytical points, resulting in a standard deviation of only ~0.3‰. The much larger error in the $^{206}Pb/^{204}Pb$ ratio is dominated by counting statistics. These measurements demonstrate the effectiveness of fast cycling to circumvent the problem of beam instabilities.

Fractionation effect is deduced from measurements on known samples. In single-stage mass spectrometry, fractionation, defined as $f = 1 - R$, where R is the measured ratio divided by the actual value, is approximately linear against the mass difference of the isotopes involved in the ratio. However, in AMS the fractionation effect can be non-linear, especially when the bouncer is operated near the limits where transmission efficiency declines rapidly.

We have used galena samples that have been characterised using thermal ion source mass spectrometry (G. Carr pers. comm. 2000) from Broken Hill (New South Wales), South Farrell Mine (Tasmania), Lennard Shelf (Western Australia) and Mt Isa (Queensland) to investigate the effect. Their respective isotopic ratio values are: $^{208}Pb/^{206}Pb = 2.2287, 2.072, 2.0663, 2.2218$; $^{207}Pb/^{206}Pb = 0.9619, 0.841, 0.82334, 0.9584$; and $^{206}Pb/^{204}Pb = 16.007, 18.57, 19.302, 16.116$. Figure 8 shows the fractionation effect for Pb isotopes for a series of measurements covering an 8-week period. Within a series of measurements, with the same accelerator setup, the fractionation factors are within the precision of the measurements. Over a longer period, with different conditions of the accelerator, a variation in the order of 1–2% was observed for all ratios. The non-linearity can be seen
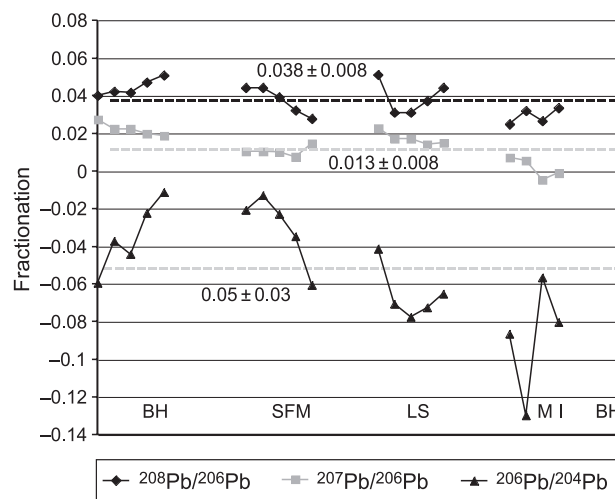
Figure 7 Repeat measurements of Pb isotopic ratios from Broken Hill galena. For the $^{207}Pb/^{206}Pb$ ratio, the standard error of individual measurement is approximately 0.7‰. The mean of the set of these measurements gave a standard error of 0.3‰. The error in the $^{206}Pb/^{204}Pb$ ratio is dominated by statistical error.

Figure 8 Fractionation effects factor for Pb isotope measurements, defined as $f = 1 - (R_{measured}/R_{standard})$, where R is the isotope ratio. The figure is a compilation from a series of measurements extending over an 8-week period for several samples of galena, with known ratios, from some Australian mines. The fractionation effect is not linear with mass difference, possibly arising from the non-linear behaviour of the transmissions through the bouncer system. The still relatively large spread results from slight differences in the tuning of the accelerator, from day to day. BH, Broken Hill, New South Wales; SFM, South Farrell Mine, Tasmania; LS, Lennard Shelf, Western Australia; MI, Mt Isa, Queensland.

where the f (208/206) is more than twice f (207/206) and appears unrelated to f (206/204). The variation observed may be attributable to the slightly different condition of the transmission through the accelerator, or in turn it may be due to the extraction of the secondary ions, including effects of different sample conductivity. Experiments are in progress to mitigate against these effects.

Sulfur isotopes

Sulfur isotope measurements present another suitable application of AUSTRALIS because of the common interference of the $^{32}S^-$ by the ubiquitous O_2^- ions, as well as $^{34}S^-$ by possible hydride ions $^{33}SH^-$ or $^{32}SH_2^-$ from residual air in the vacuum or the host mineral itself. Oxygen interference requires approximately 1800 mass resolution, while the hydrides can be resolved with mass resolution in the 2000–3000 range. There may be other interference from the matrix itself, for example, doubly charged ^{64}Zn ions in sphalerite that require high resolution. With AMS, high resolution is not necessary as these molecules are eliminated at the high-energy side. The advantage of AMS for the low-mass region may not be as significant, as modern ion probes (SHRIMP, IMS1270, Cameca 4f) have been used successfully to resolve interference problems in S (Eldridge *et al.* 1987; Riciputi 1996; Patterson *et al.* 1997) and O isotope measurements (Riciputi *et al.* 1998; McKeegan *et al.* 1996) using high resolution and extreme energy-filtering techniques. The latter technique is necessarily a low-efficiency technique.

To investigate the efficacy of sulfur isotope measurements using AUSTRALIS, we have chosen a selection of sulfides (galena, pyrite, chalcopyrite and sphalerite) as test samples. In the case of galena, it is possible to select the PbS$^-$ ions, which are quite prolific, but we eventually concentrated on using the S$^-$ ions, being the most intense peak in the mass spectrum. Figure 9 shows a typical mass spectrum for sulfur, showing the mass 32, 33 and 34 peaks measured at the low-energy mass spectrometer side and in
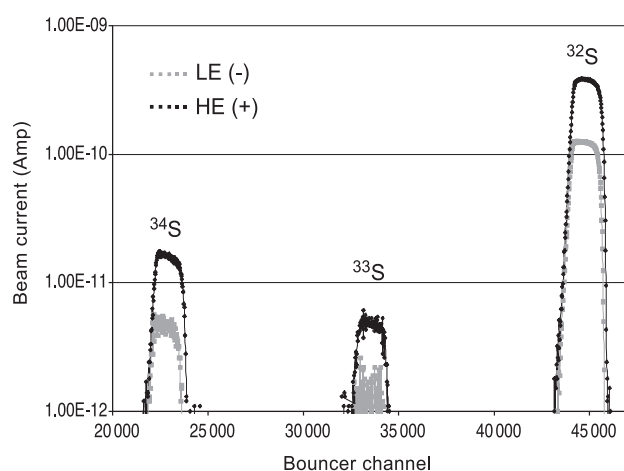
the Faraday cup at the high-energy end of the accelerator. The magnitude of hydride interference can be judged from the high $^{33}S/^{32}S$ ratio, compared to the expected value of 0.75%. Figure 10 shows the composite mass spectrum of sulfur isotopes (2+ charge state) measured in the Faraday cup after the high-energy spectrometer (as current) and in the ion counter after additional electrostatic analysis.

The beam intensity is sufficient for detection with the Faraday cup. However, the slow integrating time of the electrometers does not allow fast cycling and we have to revert to the ion counter for isotope ratio measurements. These were carried out with a more attenuated injected beam in order to keep the maximum count rate at approximately one million counts per second for minimal dead-time correction. Magnetic analysis can result in ambiguity [e.g. $^{32}S^{2+}$ would have almost the same magnetic rigidity (mE/q^2) as $^{16}O^+$, which originates from injected $^{16}O_2^-$ molecular ions, showing as the minor peak near the ^{32}S peak]. The electrostatic analysis removes this contribution as can be seen in the bottom figure in Figure 10.

The reproducibility of the results is illustrated in Figure 11, showing two isotopic ratio measurements from the same sample. The obtained ratio is out by ~10% from the expected ratio of 0% for this Broken Hill sample,
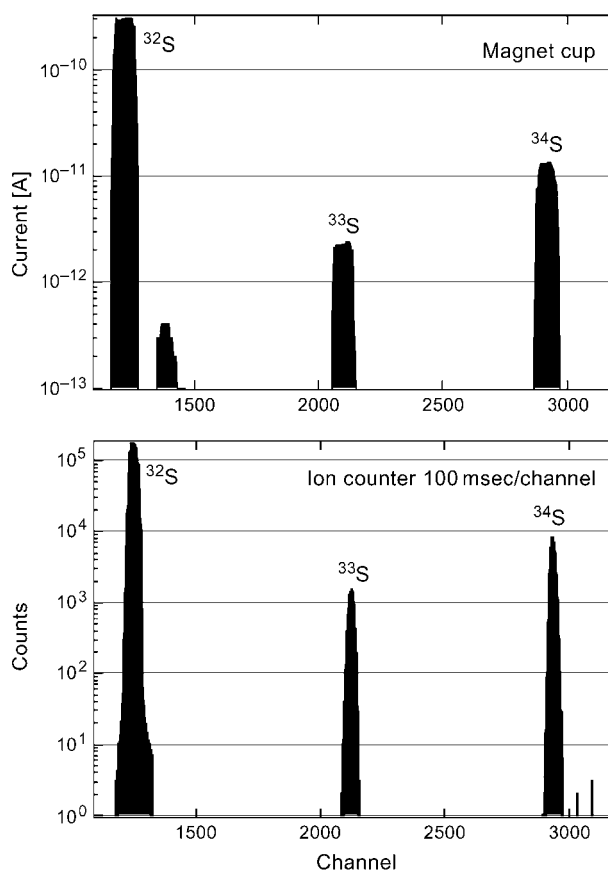
Figure 9 Mass spectrum of sulfur measured in the Faraday cups as negative current (grey points) at the low energy (LE) and as positive current (black) at the high energy (HE) side. The higher current at HE reflects the charge multiplication as a result of charge conversion from singly charged negative ions to multiply charged positive ions.

Figure 10 Composite mass spectrum of sulfur isotopes at the high-energy side, from their respective injection of S$^-$ ions. The spectra were measured before electrostatic analysis in the high-energy magnet Faraday cup, and after analysis in the high-energy ion counter. The minor peak near the $^{32}S^{2+}$ peak is $^{16}O^{1+}$ from injected $^{16}O_2^-$, which is not observed in the ion counter being filtered out by electrostatic analysis.

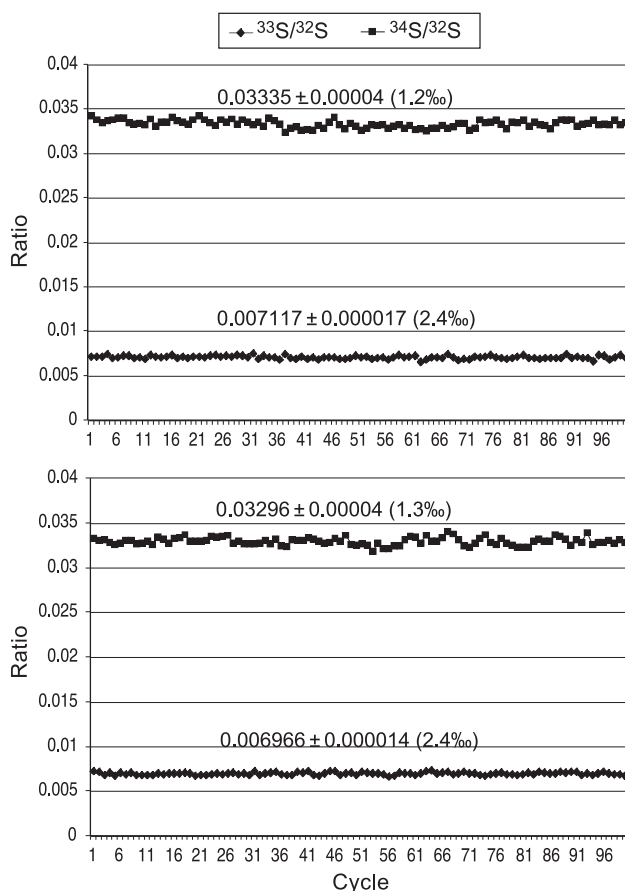**Figure 11** The results of two $^{34}S/^{32}S$ measurements from the same sample, showing good reproducibility. The obtained ratio shows a significant discrepancy with the expected ratio of 0.045 for δ_{34} = 0‰ for this Broken Hill galena sample. The instrumental fractionation is large because of the large relative mass difference.

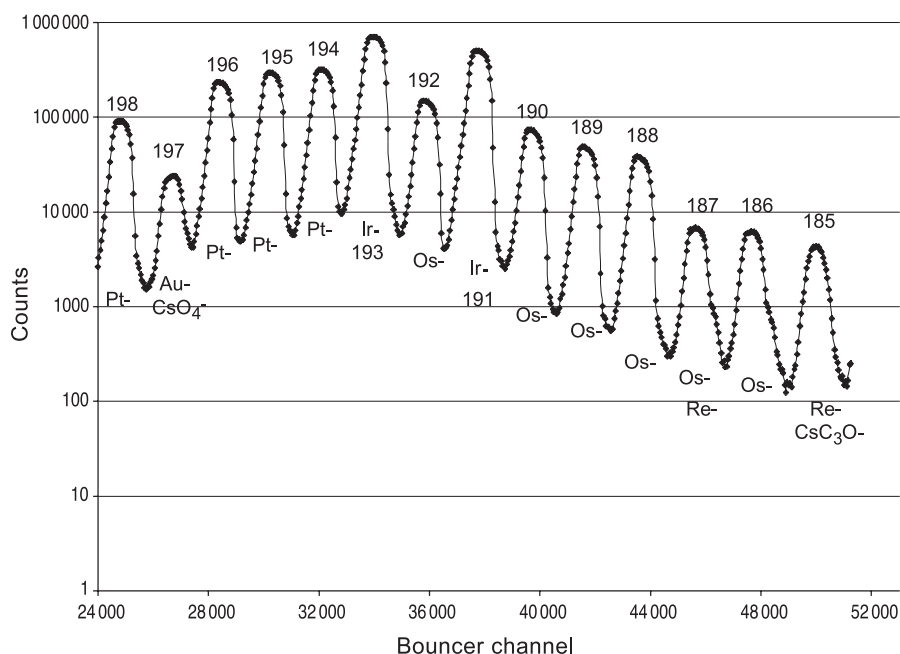indicative of the extent of the instrumental fractionation effect. This discrepancy is expected in view of the large relative mass range (6.2%) in S isotope measurements. In the case of Pb isotopes, the instrumental fractionation effect was negligible due to the lower relative mass range (1.9%). These deviations are constant for a given isotopic system and are corrected by measurements against standards.

The large contrast of the count rates between ^{34}S and ^{32}S makes them prone to error due to variation in dead-time correction in the counter. Improvement of the results can be obtained with measurement against the ^{33}S isotope.

Osmium isotopes

AUSTRALIS presents two advantages for *in situ* Os isotope measurements. It eliminates the problem of possible hydride interference (e.g. ^{187}Os by ^{186}OsH and ^{188}Os by ^{187}OsH), and ^{187}Re isobaric interference is suppressed because Os$^-$ is approximately 200-fold more prolific than Re$^-$. Figure 12 shows the low-energy mass spectrum from an osmiridium sample in the mass region of interest covering the Re, Os, Ir, Au and Pt isotopes. The sample contains a significant amount of Pt (~7%), and with the higher ionisation yield compared to Ir and Os, the peaks are prominent. The mass 185 and mass 197 peaks contain contributions due to the primary beam and residual air in the vacuum, namely the $^{133}Cs^{12}C_3O^-$ and $^{133}CsO_4^-$ ions respectively, and any hydride ions would be unresolved. These molecules are of no consequence at the high-energy end because they are destroyed during acceleration. The spectrum was obtained with an intrinsic mass resolution of ~1000 and with the image slits widened to achieve flat-topped transmission. Figure 13 shows the composite mass spectrum for the 4+ ions obtained for 1.5 MV terminal voltage, at the high-energy end using the ion counter, for the corresponding injected isotopes. The high-energy magnet is set at a fixed field to pass $^{193}Ir^{4+}$ from $^{193}Ir^-$.

Figure 12 The low-energy mass spectrum from an osmiridium sample in the mass region of interest covering the Re, Os, Ir, Au and Pt isotopes. The mass 185 and mass 197 contain contributions from the beam and residual CO and CO_2 in the vacuum chamber, namely $^{133}Cs^{12}C_3O^-$ and $^{133}CsO_4^-$, respectively.

Because the bouncer system is limited to scanning only eight isotopes, the full range of the Os–Au isotopes has to be measured in two passes, with overlap on Ir. These measurements were carried out with low intensity of the Cs beam, to manage the count rate in the detector below one million counts per second. This was achieved by turning off the Cs reservoir heater, as well as by reducing the source slits to 20 μm.

With a normal beam intensity and normal slit opening of 500 μm, the high efficiency resulting from not requiring high resolution enables measurements of isotopes at low concentration levels. This is illustrated by the measurement of an iron meteorite HOBA (Buchwald 1975), which contains PGE at a level of several ppm, shown superimposed in Figure 13.

Figure 14 shows the spectrum from the Canyon Diablo meteorite, indicating reasonable count rate for the 187 and 188 isotopes for dating purposes, using the 4+ ions. In this sample there was no detectable mass 185 peak. The result demonstrates the possibility of routine *in situ* measurements of Os isotopes in low-level samples, at least in extraterrestrial samples. For applications on terrestrial samples, especially crustal material, relative enrichment of Re over Os may result in significant [187]Re in the Os peak necessitating appropriate correction. This may detract from the precision attainable, for example, in dating sulfide deposits using chalcopyrite. For Re/Os determination, Re can be obtained from the ReO$^-$ ions, which are more prolific than the Re$^-$ beam, whereas Os can be obtained from Os$^-$ being more prolific than OsO$^-$ ions.

For the mass range covered by these elements, it is possible to use the 3+ ions, which have magnetic rigidity just below the maximum power of the present magnet.
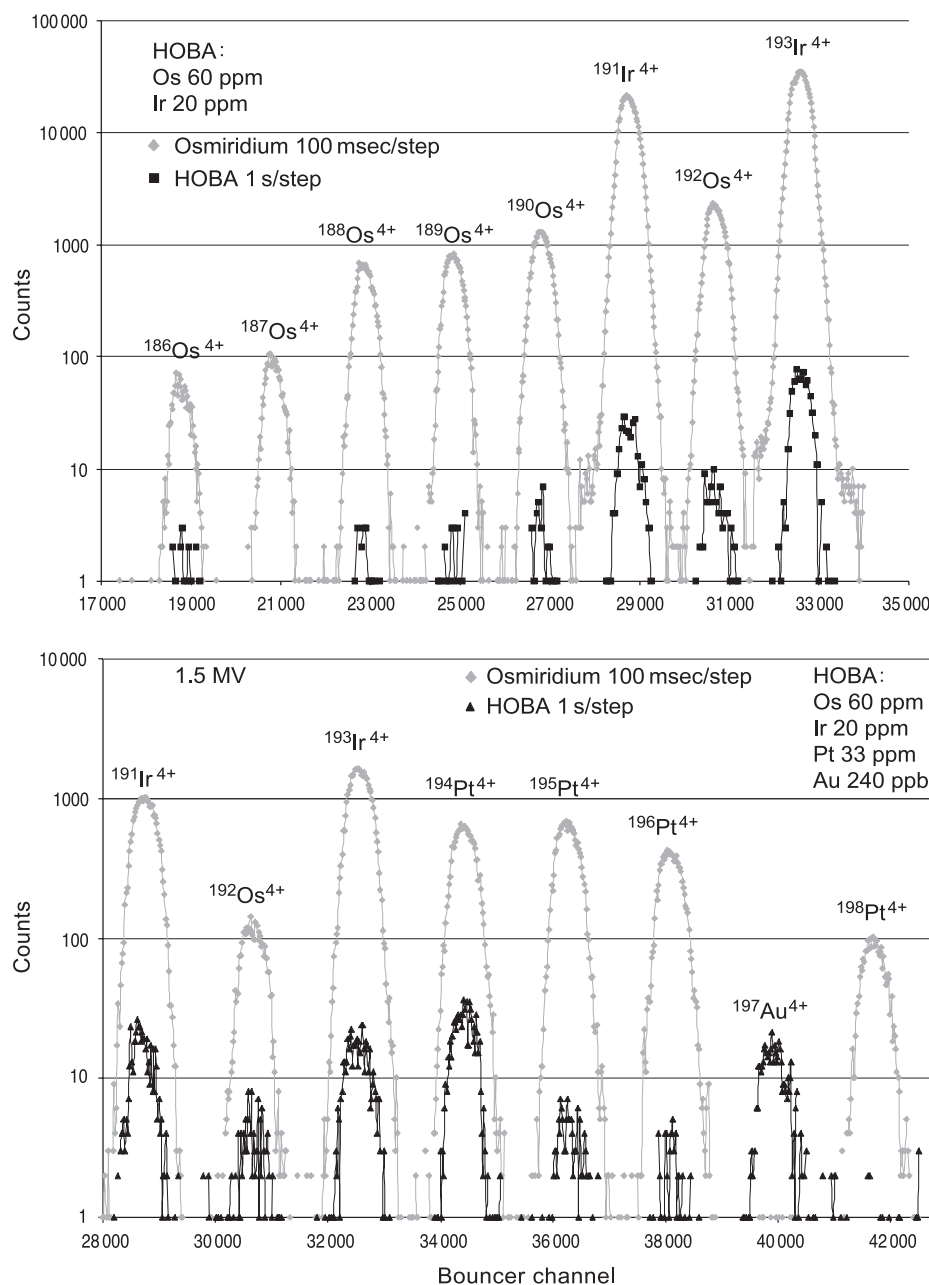

Figure 13 The composite mass spectra from osmiridium (grey points) for the 4+ ions obtained for 1.5 MV terminal voltage, at the high-energy end using the ion counter, for the corresponding injected isotopes. The high-energy magnet is set at a fixed field to pass [193]Ir^{4+} from [193]Ir$^-$ and the high-energy bouncer scanned to cover approximately four mass units on either side. Two separate passes are required to cover the range of isotopes shown. Superimposed in these figures (black points) are the spectrum from an iron meteorite (HOBA) containing PGE at several ppm level.

A 10-fold yield was obtained over the 4+ ions, which will improve detection at lower levels of concentration.

Trace-element analysis

Although the advantages of AUSTRALIS accrue mainly in isotope geology applications, the elimination of interference leads to ultra-sensitivity in many trace-element measurements. The sensitivity is not monotonic across the periodic table because of the large variation in ionisation efficiency, but in favourable cases, sub-ppb detection limits can be achieved. Such is the case for heavy PGE and Au,

which are prolific negative ion producers. Figure 15 shows a mass spectrum obtained for a NiS fire-assay bead prepared from SARM-7 standard for PGE trace-element measurements (Steele *et al.* 1975), superimposed on the osmiridium spectrum. The bead only results in a 1.1 preconcentration, but provides a good conducting matrix for the analysis. The Au peak is very prominent, reflecting the high ionisation yield of Au. In this sample, the expected Au concentration is 310 ppb, and the high count rate of ~300 counts/s was obtained with ~20 nA primary Cs$^+$ beam. This result demonstrates the high sensitivity for Au detection at a sub-ppb level.
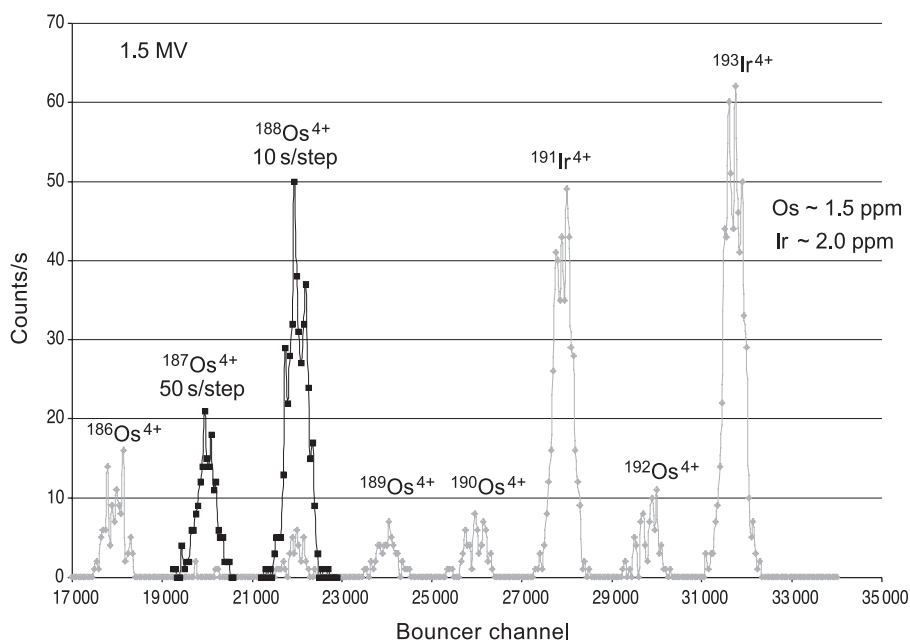

Figure 14 Mass spectrum from the Canyon Diablo meteorite showing the Os isotopes 187 and 188, demonstrating the possibility of routine isotopic ratio measurement from low-level Os samples.
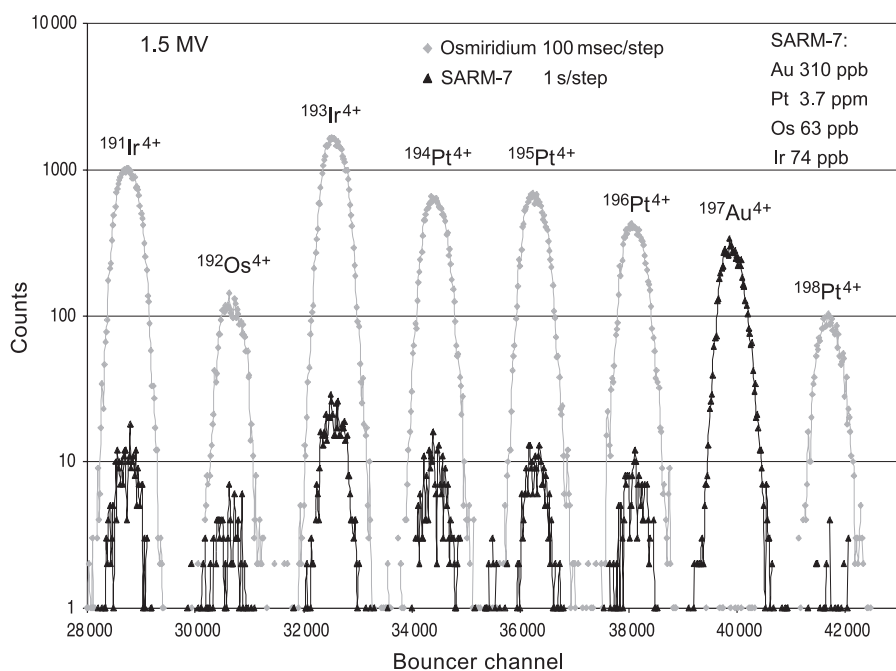

Figure 15 Mass spectrum obtained from SARM-7 (black points), a standard for trace PGE and Au measurements, against that obtained from osmiridium (grey points) for mass calibration. The sample was fused into a NiS matrix, with a preconcentration factor of 1.1. The Au concentration is 310 ppb, and the spectrum clearly shows that it is well above the detection limit.

CONCLUSIONS

A microbeam AMS system designed mainly for *in situ* geochronology applications has been constructed. It is essentially double mass spectrometry, in which the first stage is an ion microprobe and an accelerator interposed between the two mass spectrometer systems acting as a molecular disintegrator that eliminates most mass interference. Fast sequential isotope switching method is used to achieve high precision in isotopic ratio measurements. In tests on Pb isotopes, reproducibility within a series of measurements and precision as good as 0.03% has been achieved. Elimination of molecular interference is demonstrated in these measurements from galena. Initially, fractionation effects varied within 2% over longer periods for Pb, and were larger for S isotopes, but this has now been significantly improved to better than 0.5% after all the critical beam-transport elements were put under computer control. High sensitivity was demonstrated in the Os isotope measurements in iron meteorite and sulfides. The trace-element capability was demonstrated in Au measurement, where sub-ppb detection sensitivity was achieved in NiS. The system paves the way for applications in isotope geology previously not feasible using the *in situ* method.

REFERENCES

Buchwald V. 1975. *Handbook of Iron Meteorites*. University of California Press, Berkeley.

Compston W., Williams I. S. & Clement S. W. J. 1982. U–Pb ages within single zircons using a sensitive high mass-resolution ion microprobe. *In*: *30th Annual Conference of the American Society of Mass Spectrometry, Honolulu*, pp. 593–595.

Eldridge C. S., Compston W., Williams I. S., Walshe J. L. & Both R. A. 1987. In-situ microanalysis for $^{34}S/^{32}S$ ratios using the ion microprobe SHRIMP. *International Journal of Mass Spectrometry and Ion Processes* **76**, 65–83.

McKeegan K. D., Leshin L. A., Russell S. S. & MacPherson G. J. 1996. In-situ measurement of oxygen isotopic anomalies in type B Allende CAI. *Meteoritic and Planetary Science* **31**, A86–A87.

Patterson B. A., Riciputi L. R. & McSween H. Y. Jr 1997. A comparison of sulfur isotope ratio measurement using two ion microprobe techniques, and application to troilite in ordinary chondrites. *Geochimica et Cosmochimica Acta* **61**, 601–610.

Reed S. J. B. 1989. Ion microprobe analysis—a review of geological applications. *Mineralogical Magazine* **53**, 3–24.

Reed S. J. B. 1990. Recent developments in geochemical microanalysis. *Chemical Geology* **83**, 1–9.

Riciputi L. R. 1996. A comparison of extreme energy filtering and high mass resolution techniques for the measurement of $^{34}S/^{32}S$ ratios by ion microprobe. *Rapid Communication in Mass Spectrometry* **10**, 282–286.

Riciputi L. R., Patterson B. A. & Ripperdam R. L. 1998. Measurement of light stable isotope ratios by SIMS: matrix effects for oxygen, carbon and sulfur isotopes in minerals. *International Journal of Mass Spectrometry and Ion Processes* **178**, 81–112.

Sie S. H., Niklaus T. R. & Suter G. F. 1997. Microbeam AMS: prospects of new geological applications. *Nuclear Instruments and Methods* **B123**, 112–121.

Steele T. W., Levin J. & Copelowitz I. 1975. *The Preparation and Certification of a Reference Sample of a Precious Metal Ore*. Report **1696**. National Institute of Metallurgy, Johannesburg.

Walder A. J., Abell I. D., Platzner I. & Freeman P. A. 1993. Lead isotope measurement of NIST610 glass by laser ablation inductively coupled plasma mass spectrometry. *Spectrochimica Acta* **48B**, 397.